

Particles II

Access the latest eBook →

11

Advanced
Optical Metrology

Particles II



EVIDENT
OLYMPUS

WILEY

Impact on Biological Systems and the Environment

This eBook is dedicated to the research of Professor David Wertheim.

In collaboration with various groups, Professor Wertheim uses confocal microscopy to analyse the impact of different types of particles on human health and the environment, with a focus on human health-hazardous particles detected with solid-state nuclear track detectors (SSNTD). Download for free, today.

EVIDENT
OLYMPUS

WILEY

Single-Source Bismuth (Transition Metal) Polyoxovanadate Precursors for the Scalable Synthesis of Doped BiVO₄ Photoanodes

Haijiao Lu, Virgil Andrei, Kellie J. Jenkinson, Anna Regoutz, Ning Li, Charles E. Creissen, Andrew E. H. Wheatley, Hongxun Hao, Erwin Reisner,* Dominic S. Wright,* and Sebastian D. Pike*

Single-source precursors are used to produce nanostructured BiVO₄ photoanodes for water oxidation in a straightforward and scalable drop-casting synthetic process. Polyoxometallate precursors, which contain both Bi and V, are produced in a one-step reaction from commercially available starting materials. Simple annealing of the molecular precursor produces nanocrystalline BiVO₄ films. The precursor can be designed to incorporate a third metal (Co, Ni, Cu, or Zn), enabling the direct formation of doped BiVO₄ films. In particular, the Co- and Zn-doped photoanodes show promise for photoelectrochemical water oxidation, with photocurrent densities >1 mA cm⁻² at 1.23 V vs reversible hydrogen electrode (RHE). Using this simple synthetic process, a 300 cm² Co-BiVO₄ photoanode is produced, which generates a photocurrent of up to 67 mA at 1.23 V vs RHE and demonstrates the scalability of this approach.

such as BiVO₄, which possess appropriate band positions for the oxidation of water, show promise as the light-absorbing photoanode within a photoelectrochemical cell.^[2] The bandgap of BiVO₄ allows absorption of a significant portion of visible light, giving a theoretical solar-to-hydrogen efficiency of 9% (maximum photocurrent density = 7.5 mA cm⁻²).^[3] Indeed, BiVO₄ has been utilized in state-of-the-art tandem photoelectrochemical devices, sometimes referred to as “artificial leaves,”^[4] with monoclinic scheelite BiVO₄ established as the most effective polymorph for photoanodes.^[2c,d] Doping,^[5] nanostructuring,^[4b,6] heterojunction formation,^[7] and the addition of oxygen evolution catalysts (OECs)^[6,8] are

employed to remediate the low carrier diffusion lengths associated with BiVO₄,^[9] which reduce efficiency due to accumulation and recombination of charge carriers.^[10]

Recent reports have established efficient BiVO₄ photoanodes utilizing these strategies,^[2a,d,4b,d,11] but state-of-the-art materials have normally only been produced on small scales (e.g., <2.25 cm²)^[2d] and require complex fabrication techniques. The scalable deposition of BiVO₄ thin films onto conductive surfaces remains an important target.^[2d,11] Examples of larger BiVO₄ films are rare, however, 35 cm² films have been produced by sputtering techniques.^[12] Current synthetic routes include chemical vapor deposition^[13] and electrochemical deposition,^[4b,6] however, solution routes are particularly attractive due to their simplicity and potential for scale up. Precursors for solution preparation include inorganic salts and/or metal-organic precursors such as Bi(NO₃)₃^[4a,c,d] or Bi(2-ethylhexanoate)₃^[11] with VO(acac)₂ (acac = acetylacetonate),^[4a,c,d] VO(OR)₃ (R = Et, OⁱPr),^[11] VCl₃,^[14] or NH₄VO₃,^[15] to which precursors for doping may also be added.^[3,4c] Spray pyrolysis or drop casting/spin coating followed by an annealing step can transform these precursors into BiVO₄.^[2a,c,3] A challenge when using a mixture of soluble precursors is the even distribution of molecules and prevention of phase separation upon drying, which can result in differing morphologies or compositions across the film after calcination; especially relevant when scaling the process. For example, spin-coating Bi(NO₃)₃ and VO(acac)₂ produced a nonuniform 6 cm² film, with the central 1 cm² giving twice the photocurrent density compared to that of the whole plate.^[16]

Converting solar energy into hydrogen by the splitting of water or the conversion of anthropogenic CO₂ into fuels coupled to water oxidation are attractive solutions to energy production and storage issues.^[1] Currently, a major obstacle to the practical synthesis of solar fuels is the unfavorable kinetics of the water oxidation reaction and the access to materials that can rapidly oxidize water is therefore a key requirement. Semiconductors

H. Lu, V. Andrei, K. J. Jenkinson, N. Li, C. E. Creissen, Dr. A. E. H. Wheatley, Prof. E. Reisner, Prof. D. S. Wright, Dr. S. D. Pike
Department of Chemistry
University of Cambridge
Lensfield Road, Cambridge CB2 1EW, UK
E-mail: er376@cam.ac.uk; dsw1000@cam.ac.uk; sp842@cam.ac.uk

H. Lu, Prof. H. Hao
School of Chemical Engineering and Technology
Tianjin University
Tianjin 30072, China
Dr. A. Regoutz
Department of Materials
Imperial College London
Exhibition Road, London SW7 2AZ, UK

 The ORCID identification number(s) for the author(s) of this article can be found under <https://doi.org/10.1002/adma.201804033>.

© 2018 The Authors. Published by WILEY-VCH Verlag GmbH & Co. KGaA, Weinheim. This is an open access article under the terms of the Creative Commons Attribution License, which permits use, distribution and reproduction in any medium, provided the original work is properly cited.

DOI: 10.1002/adma.201804033

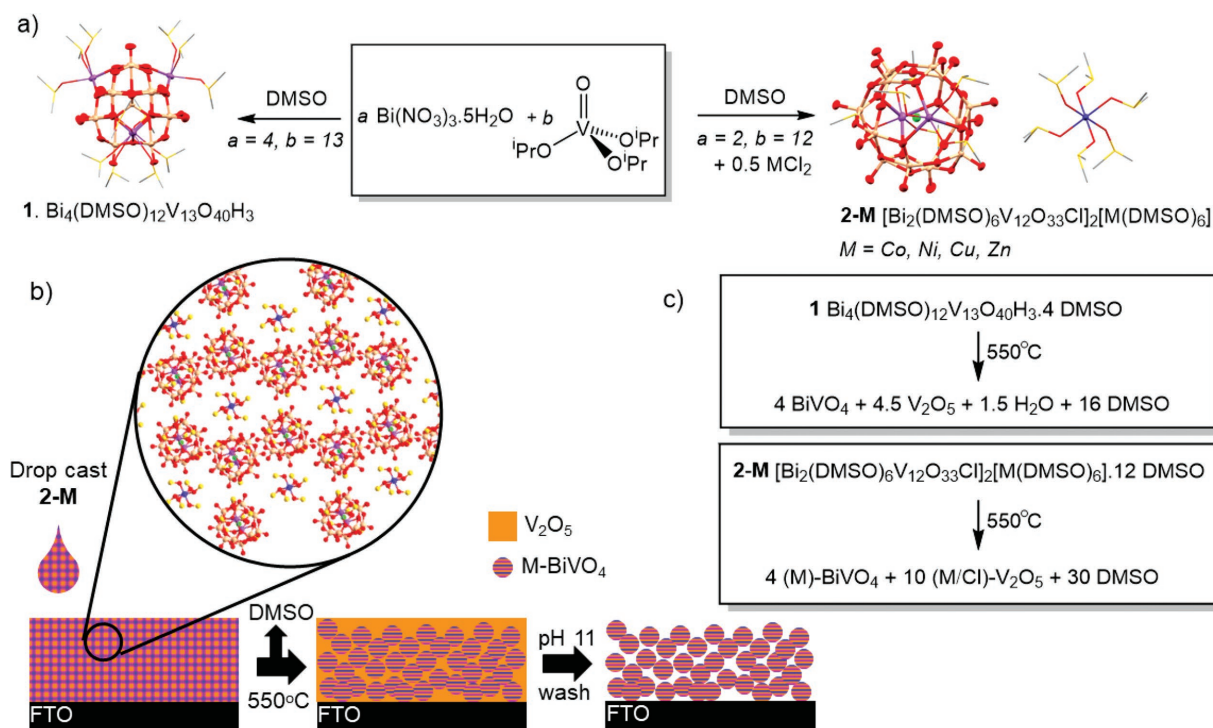


Figure 1. a) Synthesis of **1** and **2-M**, solid-state structures from X-ray crystallography are shown (hydrogen atoms omitted for clarity, DMSO ligands shown in stick form, structure of **2-Co** is representative of all **2-M**, one anion shown only). Colors, O = red, V = pale orange, Bi = purple, Cl = green, Co = blue, C = gray, S = yellow. b) Synthesis procedure for preparation of FTO|(M)-BiVO₄ photoanodes via drop casting of SSP **2-M** followed by annealing and washing (zoomed image: solid-state lattice of **2-Co** once solution has dried, carbon atoms omitted for clarity). c) Thermal decomposition equations for **1** or **2-M** to give metal oxide products.

The use of a single-source precursor (SSP) overcomes issues with phase separation and ensures a consistent film prior to annealing.^[17] In this work, SSPs consisting of Bi_xV_yO_z molecular clusters ligated only by dimethylsulfoxide (DMSO, b.p. 189 °C) are utilized to form nanostructured thin films of BiVO₄ on fluorine-doped tin oxide (FTO) substrates. The SSPs are synthesized straightforwardly, in a one-step process from commercially available starting materials. Furthermore, SSPs incorporating a dopant metal atom (M = Co, Ni, Cu, Zn) can be obtained, enabling direct production of doped BiVO₄ (M-BiVO₄). All M-BiVO₄ films show good photoactivity and may be produced on a large scale (e.g., 300 cm²). This process promises to allow the fabrication of real world devices, including multilayer tandem systems.^[8b]

Molecular SSPs to BiVO₄ were inspired by reports by Streb and co-workers, who reported the synthesis of bismuth polyoxovanadate clusters, Bi₄(DMSO)₁₂V₁₃O₄₀H₃ (**1**) and [Bi₂(DMSO)₆V₁₂O₃₃Cl]₂[NBu₄]₂ (**2-NBu₄**).^[18] Previously, these complexes were prepared from (nBu₄)₃(H₃V₁₀O₂₈) and Bi(NO₃)₃ (+NaCl, for **2-NBu₄**), but in our approach, the synthesis is simplified by employing commercially available VO(OⁱPr)₃ (Figure 1). SSP **1** is prepared directly from the stoichiometric reaction of VO(OⁱPr)₃ with Bi(NO₃)₃·5H₂O in DMSO. The vanadium precursor is highly water sensitive and is hydrolyzed during this reaction by the water of crystallization of the bismuth salt. Upon introducing a third metal to the reaction mixture, as MCl₂ (M = Co, Ni, Cu, Zn), a series of salts was prepared with formula [Bi₂(DMSO)₆V₁₂O₃₃Cl]₂[M(DMSO)₆] (**2-M**). Crystalline **1** or **2-M**

are obtained by slow diffusion of ethyl acetate into the DMSO solutions (isolated crystalline yields, **1** = 53%, **2-M** 57–70%).

Compounds **1** and **2-M** were characterized by single-crystal and powder X-ray diffraction (XRD), elemental analysis, UV/vis-spectroscopy, X-ray photoelectron spectroscopy (XPS), thermogravimetric analysis (TGA), and Fourier-transform infrared (FTIR) spectroscopy (Figures S1–S9 and Tables S1–S4, Supporting Information), the data for **1** were consistent with the previous report.^[18] All **2-M** are isostructural and contain 12 molecules of DMSO in the crystal lattices. The oxidation state of M was confirmed as +2 by a combination of XPS, electronic absorption spectroscopy, and by a Jahn-Teller distortion in the solid-state structure in the case of **2-Cu** (Figures S7 and S5 and Table S2, Supporting Information). TGA under N₂ showed complete loss of DMSO (and water for **1**), while under air a slightly reduced mass loss occurred (Table S4, Supporting Information). The latter potentially indicates some retention of carbon residues as supported by the darkening of the samples; this darkening is removed by washing (see later).

BiVO₄ or M-BiVO₄ films were prepared by drop-casting the precursor solutions (3.6 × 10⁻³ M **1** or **2-M** in DMSO, 40 μL cm⁻² per layer) onto FTO-coated glass before annealing by ramping the temperature to 550 °C (Figure 1). The thermal degradation requires loss of DMSO and water, but no other organics need to be removed, in contrast to the two previously reported complexes which can be decomposed to BiVO₄ (neither of these have been reported to produce photoanodes).^[19] The produced films were washed with 0.2 M NaOH solution to remove V₂O₅

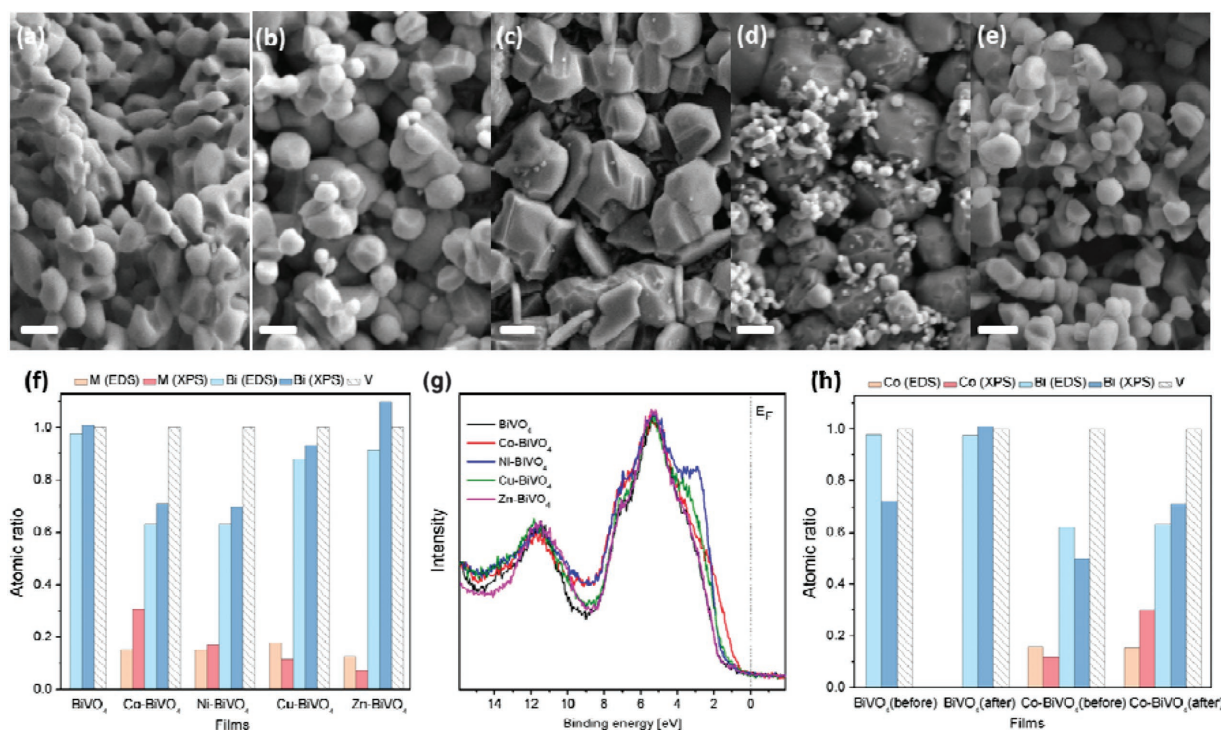


Figure 2. Characterization of M-BiVO₄ films (a–g after use as a photoanode) SEM images of: a) BiVO₄, b) Co-BiVO₄, c) Ni-BiVO₄, d) Cu-BiVO₄, e) Zn-BiVO₄, all scale bars indicate 500 nm. f) Bulk and surface atomic ratios from EDS and XPS respectively (V is set to be 1). g) XPS valence band spectra of (M-)BiVO₄ photoanodes, h) Bulk and surface atomic ratios from EDS and XPS respectively (V is set to be 1) of BiVO₄ and Co-BiVO₄ before and after photoelectrochemical treatment.

and other potential impurities such as metal chlorides.^[15,20] Thin films comprising multiple layers (up to 6) were prepared by repeating the process, in order to maximize the photocurrent. The thickness of Co-BiVO₄ increases by ≈150–250 nm for each new layer (Figure S11, Supporting Information). The simplicity of the method, which requires only a furnace, allows the simultaneous preparation of multiple medium or large-scale photoanode panels (see below).

All of the undoped and doped films were characterized by powder XRD and diffuse reflectance UV–vis spectroscopy, which indicated the formation of monoclinic scheelite BiVO₄ with bandgaps of 2.4–2.5 eV (Figures S10 and S32, Supporting Information). During annealing, the SSPs decompose to form two separate phases (a type III SSP),^[17a,21] e.g., BiVO₄ and V₂O₅ (Figure 2a–e).^[20] Scanning electron microscopy (SEM) with energy-dispersive X-ray spectroscopy (EDS) conducted before the washing process indicated the presence of large rods amongst smaller particles, with the rods composed mainly of V and O (Figures S26 and S27, Supporting Information). Crystalline V₂O₅ was not identified by XRD (Figure S10c, Supporting Information), supporting the existence of an amorphous vanadium oxide phase.

Further characterization (including SEM and XPS) of films was conducted both before and after their use as photoanodes (see later). XPS and EDS confirmed the loss of all Cl and S from the films and that the 2p core levels for dopant M were very similar to those in 2-M (Figures S28 and S7, Supporting Information). Therefore, Co and Ni are identified in the +2 oxidation state, but this could not be unambiguously determined for Cu and Zn. The morphology and bulk composition of the

films were examined by SEM and EDS, complementing the surface composition analysis by XPS. The undoped BiVO₄ film is composed of ≈300 nm particles, with the expected 1:1 bulk ratio of metals, indicating successful removal of all V₂O₅ by washing (Figures S14 and S15, Supporting Information). The surface is initially V rich, but the surface V:Bi ratio becomes 1:1 after photoelectrochemical treatment (Figure 2h and Figure S30, Supporting Information). The morphology also appears slightly less monodisperse after use as a photoanode, suggesting a slight degradation of the surface structure during use (Figure S12 vs Figure S14, Supporting Information). Zn-doping occurs uniformly throughout the film and leads to slightly larger ≈400 nm particles that contain a V:Bi:Zn ratio of 1:0.91:0.13 (ratios ± 0.01) (Figure 2e–f and Figures S24 and S25, Supporting Information), which indicates replacement of 1 Bi³⁺ by 1.5 Zn²⁺. Co doping creates a greater particle size dispersity (≈200–500 nm, Figure 2b, Figures S18 and S19, Supporting Information) and while EDS suggests that Co is distributed throughout the material, XPS identifies that the surface becomes Co enriched after use as a photoanode (approximately twice the concentration of Co in the surface (≈6–9 nm) compared to the bulk, Figure 2f,h and Figure S31, Supporting Information). Despite the mobility of Co, the morphology of Co-BiVO₄ is not greatly affected during photoelectrochemical testing (Figure S16 vs Figure S18, Supporting Information). This is particularly interesting as various Co-based surface layers, which may act as OECs and/or suppress surface recombination, are known to greatly enhance water oxidation efficiency and photoanode stability, and an accumulation of Co on the BiVO₄ surface is

therefore likely to improve catalytic performance.^[6,10] In the cases of Cu and Ni doping, multiple phases are identified by EDS point scans: for Cu, small particles (≈ 150 nm) of Cu-doped BiVO_4 are located alongside larger (≈ 700 nm) particles which appear to be undoped BiVO_4 (Figures S22 and S23, Supporting Information); for Ni, large plates ($\approx 600 \times 600 \times 100$ nm) of a Ni rich vanadium oxide phase are located alongside particles consisting mainly of BiVO_4 (Figures S20 and S21, Supporting Information). For both Co and Ni doping a significant excess of V is observed, suggesting incorporation of a secondary phase of amorphous (M-doped) vanadium oxide, which is sustained in spite of the washing process.

The electronic structure of the (M)- BiVO_4 films was examined by XPS (Figure 2g) and the valence band (VB) of the BiVO_4 photoanode shows the expected structure for BiVO_4 .^[22] The addition of Zn does not seem to have an influence on the structure of the VB, with both materials displaying VB_{max} to E_{F} separation ($\Delta_{\text{VB-EF}}$) of ≈ 1.6 eV, as calculated from fits to the VB maximum (VB_{max}) and the background (Figure S29, Supporting Information). In contrast, the other three metals, Co, Ni, and Cu, all introduce extra structure to the VB, particularly the states closest to the Fermi energy E_{F} (Figure 2g). XPS is particularly sensitive to the surface structure and these changes are best explained by the presence of the extra phases or surface structuring, evidenced by a shift in $\Delta_{\text{VB-EF}}$ for Co- BiVO_4 before and after photoelectrochemical treatment ($\Delta_{\text{VB-EF}}$: before, 1.35 eV; after, 0.72 eV). Alongside surface analysis using XPS, the flatband potential (E_{fb}) of the bulk semiconductor films

was determined using electrochemical impedance spectroscopy (Figure S39, Supporting Information). The Mott-Schottky plots displayed a positive gradient, indicating an n-type behavior in all cases. The E_{fb} of undoped BiVO_4 (+0.04 V vs reversible hydrogen electrode (RHE)) was similar to literature values,^[6,9,11] while Co and Zn cause an anodic shift (E_{fb} vs RHE: Co- BiVO_4 , +0.22 V; Zn- BiVO_4 , +0.29 V) consistent with metals acting as p-type dopants (Bi^{3+} replaced by M^{2+}).^[15] Such a shift may result in a slightly later onset potential for these photoelectrodes. Cu- BiVO_4 ($E_{\text{fb}} = 0$ V vs RHE) displays an inversion region attributed to multiple phases or heavy dopant density (possibly from both n-type and p-type components, e.g. Cu_2O , see Figure S39d, Supporting Information).

The photoelectrochemical properties of (M)- BiVO_4 electrodes were studied by linear sweep voltammetry (LSV), cyclic voltammetry (CV) and chronoamperometry (CA) in a three-electrode configuration, using a 0.1 M potassium borate (KBi) buffer solution (pH 8.5) with 0.1 M K_2SO_4 or Na_2SO_3 , under irradiation by simulated solar light (AM1.5G filter, 100 mW cm^{-2}). The fast photooxidation of the soluble electron donor $[\text{SO}_3]^{2-}$ acts as a useful model reaction for the decoupling of the light-harvesting ability from water-oxidation catalysis. Due to negligible losses via surface charge recombination, a maximum photocurrent density (up to $1.69 \pm 0.02 \text{ mA cm}^{-2}$ at 1.23 V vs RHE for Zn- BiVO_4) and an onset potential (≈ 0.35 V vs RHE, see Figure 3a and Figure S34, Supporting Information) are observed for the M- BiVO_4 photoanodes with the optimized number of layers. The maximum photocurrent densities of M- BiVO_4 samples are 1.5–2.2 times higher

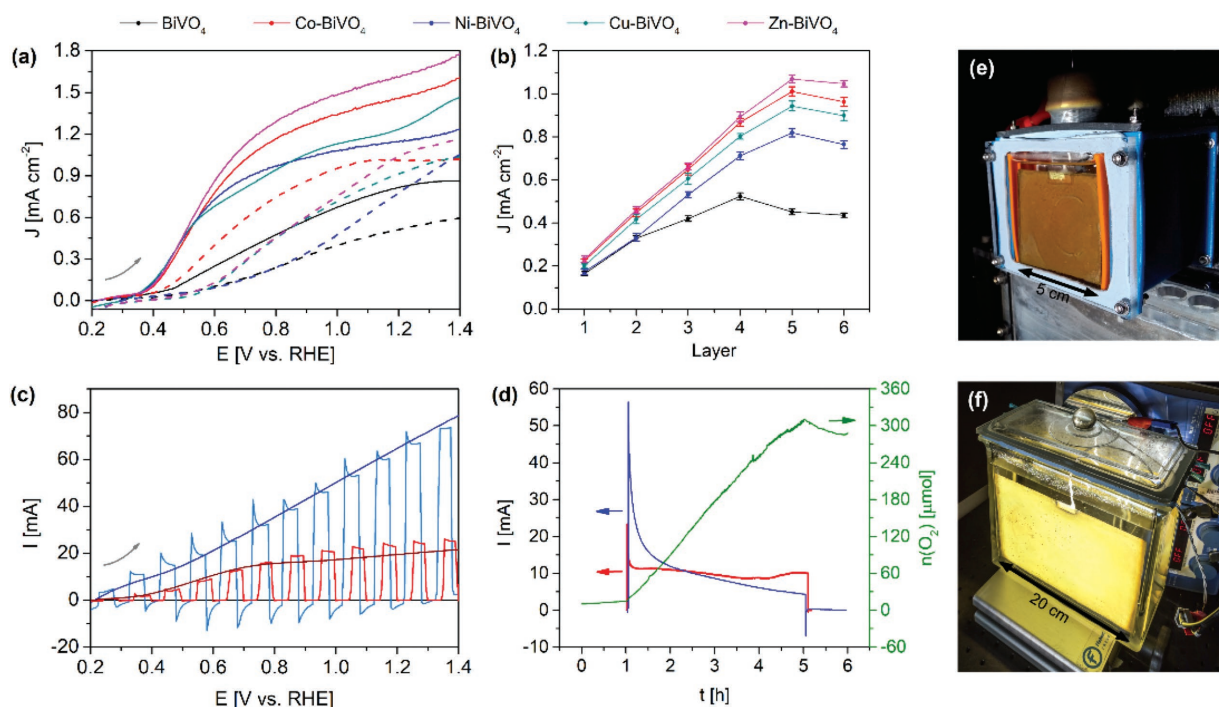


Figure 3. Photoelectrochemical performance. a) Continuous light scans of the best-performing electrodes (1 cm^2) in a 0.1 M KBi buffer (pH 8.5) with either 0.1 M Na_2SO_3 as a hole scavenger (solid lines), or 0.1 M K_2SO_4 supporting electrolyte (dashed curves). b) Dependence of the average photocurrent density (J) on the number of deposited (M)- BiVO_4 layers for Co-, Ni-, Cu-, Zn-doped and undoped 1 cm^2 BiVO_4 electrodes at 1.23 V vs RHE (0.1 M KBi, 0.1 M K_2SO_4 , pH 8.5). c) LSV scans of the 25 cm^2 (red) and 300 cm^2 (blue) electrodes, conducted in forward direction (see gray arrow) under constant and chopped back-irradiation (simulated solar light, 100 mW cm^{-2} , AM1.5G; 10 mV s^{-1} scan rate). d) 4 h stability tests of 25 cm^2 (red) and 300 cm^2 (blue) Co- BiVO_4 electrodes at 1.23 V vs RHE, and corresponding oxygen evolution trace (green) for the 25 cm^2 sample. e) Image of a $5 \times 5 \text{ cm}^2$ medium-scale electrode. f) Image of the $20 \times 15 \text{ cm}^2$ large-scale panel.

than for undoped BiVO₄ and decrease in the order Zn > Co > Cu > Ni > no doping. The photocurrent improvement may be attributed to a structural effect from the dopant metal, e.g., changes in morphology and effective surface area. Replacement of Bi³⁺ by M²⁺ with associated alteration of defect states is also known to affect charge accumulation and transport.^[15]

Photoanodes of varying thickness were tested similarly for water oxidation in the absence of [SO₃]²⁻ (Figure 3b and Figure S35, Supporting Information). The photocurrent density of undoped BiVO₄ samples increased with the number of deposition cycles, from 0.16 ± 0.01 mA cm⁻² at 1.23 V vs RHE (back-illumination) for a single layer, up to 0.52 ± 0.02 mA cm⁻² for the corresponding four-layer electrodes, presumably due to increased light absorption (Figure 3b). The result is consistent with that of unmodified BiVO₄ films prepared by reported procedures (e.g., 0.5 mA cm⁻² by sputtering,^[23] 0.6 mA cm⁻² by spray pyrolysis^[24]), although pinhole-free BiVO₄ has recently been reported to generate a photocurrent ≈2.2 mA cm⁻².^[14] A slightly lower photocurrent was observed beyond the fourth layer due to charge transport limitations (Figure 3b).^[3]

The doped electrodes showed similar behavior, reaching maximum values of 1.07 ± 0.02 (Zn), 1.01 ± 0.02 (Co), 0.94 ± 0.02 (Cu), 0.82 ± 0.02 (Ni) mA cm⁻² at 1.23 V vs RHE (back-illumination) for five-layer samples, in the same order as observed for [SO₃]²⁻ oxidation. The higher photocurrent densities from [SO₃]²⁻ oxidation (Figure 3a and Figure S34, Supporting Information) indicate a degree of charge recombination at the semiconductor–electrolyte interface during water oxidation. The photocurrent from Co-BiVO₄ samples shows an early onset potential at ≈0.4 V vs RHE and increases rapidly at low overpotentials (e.g., 0.74 mA cm⁻² at 0.8 V vs RHE, Figures S34 and S35, Supporting Information), which indicates a major role for the Co-enriched surface structure in the water oxidation catalysis. However, the highest photocurrent density, at 1.23 V vs RHE, is found for Zn doping, where the dopant may behave primarily as a structural modifier, dispersed throughout the material, rather than supplying a surface ZnO heterojunction. These results suggest that dopants can enhance water oxidation performance in different ways and introduce the possibility of more complex multidoped systems, potentially accessible by mixtures of the isostructural 2-M precursors, a tactic which could also control doping concentrations and avoid the formation of secondary phases.

To prove the feasibility of our SSP deposition technique for industrial up-scaling, three 5 × 5 cm² and one 15 × 20 cm² five-layer Co-BiVO₄ electrodes were prepared by the same procedure as the 1 cm² electrodes. Co was the chosen dopant for scale-up because it was the best performing photoanode at low overpotentials (e.g., <1 V vs RHE) and reached a similar maximum photocurrent density to Zn doping. As Figure 3c shows, both 25 (Figure 3e) and 300 cm² (Figure 3f) electrodes show high initial photocurrents of 19.8 and 66.8 mA at 1.23 V vs RHE, corresponding to current densities of 0.82 and 0.22 mA cm⁻², respectively. These absolute photocurrents are some of the largest reported to date for BiVO₄-based photoanodes. In contrast, state-of-the-art photoanodes with very high photocurrent densities are currently only fabricated and tested on small scales (e.g., <2.25 cm²) generating absolute photocurrents typically being less than 12 mA at 1.23 V vs RHE.^[2d,25]

The average photocurrent density (0.69 ± 0.23 mA cm⁻²) of three 25 cm² electrodes is comparable to that of 1 cm² samples (68% of value), indicating the overall excellent scalability and reproducibility of the deposition technique (see CV scans in Figure S36, Supporting Information). The lower current density of the 300 cm² photoanode can be mainly attributed to resistive losses due to FTO (see the linear, ohmic photocurrent behavior with the applied potential in Figure 3c, corresponding to the case of increased series resistance observed in both photovoltaics and photoelectrochemistry).^[26] In-plane potential distribution within the FTO sheet, local current densities and local pH gradient build-up may play a role in the reported decrease in photocurrent density for larger illuminated areas.^[27] However, in a practical device, additional metal fingers or metal foil substrates could be deployed to mitigate resistive losses within the transparent substrate. Gaps between individual panels in a modular device would also aid the ionic diffusion between the anodic and cathodic compartments of a complete water-splitting array, reducing pH gradient build-up.^[26a,27a,b,28]

The Co-BiVO₄ electrodes remained active for water oxidation when irradiated over 4 h, with the photocurrents either stabilizing within the first 30 min (see CA traces of 25 and 1 cm² samples in Figure 3d and Figure S37a, Supporting Information, respectively), or continuously decaying (see examples of 300 and 25 cm² electrodes in Figure 3d and Figure S37b, Supporting Information, respectively).^[12] CV scans of the 300 cm² panel after the stability test revealed large spikes under chopped irradiation indicative of increased charge recombination (Figure S38, Supporting Information).^[8a,24] The poor stability of the 300 cm² sample may be due to the uneven potential distribution caused by the sheet resistance of the large FTO plate, which may in turn favor BiVO₄ degradation. The best performing 25 cm² sample produced 271 μmol O₂ over 4 h, corresponding to a faradaic efficiency of 88% (see green oxygen evolution trace of the 25 cm² electrode in Figure 3d).

In summary, we present an inexpensive, straightforward, and scalable route to thin films of optionally doped BiVO₄, from easily synthesized SSPs composed of bismuth polyoxovanadates with 3d-metal (Co, Ni, Cu, Zn) cations. The films are ideal for use as water oxidizing photoanodes, and thin films of Co- and Zn-doped BiVO₄ show particular promise with photocurrent densities of >1 mA cm⁻² at 1.23 V vs RHE. Thermal decomposition of the SSPs at 550 °C releases DMSO and produces nanocrystalline BiVO₄ alongside amorphous V₂O₅ (which can be easily removed by washing). The surface of Co-BiVO₄ photoanodes is Co enriched, which may result in a Co-based surface OEC.

The results indicate that good performance single panels approaching practical sizes can be easily prepared using this procedure, such panels could be connected to form larger modules for commercial applications. A reduction in photocurrent density and photoanode stability is observed for the larger panels, which presents device engineering challenges for future development. From the synthetic perspective, the SSP approach can provide a technological edge, since doping can be precisely controlled at a molecular level. The straightforward synthetic route produces stable crystalline precursors, which may be transformed to films on demand. The simple solution deposition process reported should be easily adaptable for the formation of more complex nanostructured or heterojunction

photoanodes or for use in multilayer tandem photoelectrochemical devices. The ability to produce large-scale systems (e.g., 300 cm² as prepared in this work) for water splitting using simple techniques is an essential requirement for the commercialization of photochemical water-splitting technologies, and the use of soluble SSPs is an ideal strategy for producing (doped) films with excellent homogeneity on a large scale.

[CCDC 1849428–1849431 contain the supplementary crystallographic data for this paper. These data can be obtained free of charge from The Cambridge Crystallographic Data Centre via www.ccdc.cam.ac.uk/data_request/cif.]

Supporting Information

Supporting Information is available from the Wiley Online Library or from the author. The raw data that support the findings of this study are available from the University of Cambridge data repository, <https://doi.org/10.17863/CAM.27056>.

Acknowledgements

The authors thank the following for financial support: China Scholarship Council (H.L.), the Cambridge Trusts (Vice Chancellor's Award) and the Winton Programme for the Physics of Sustainability (V.A.), EPSRC (EP/J500380/1, K.J.J.) A*STAR, Graduate Scholarship (Overseas) (N.L.), Imperial College Research Fellowship (A.R.), EPSRC NanoDTC in Cambridge (EP/L015978/1;C.E.C.), Christian Doppler Research Association and the OMV Group (E.R), Herchel Smith Research Fund (S.D.P).

Conflict of Interest

The authors declare no conflict of interest.

Keywords

BiVO₄, doping, polyoxovanadate, single-source precursor, water oxidation

Received: June 25, 2018
Revised: August 12, 2018
Published online: October 4, 2018

- [1] J. K. Stolarczyk, S. Bhattacharyya, L. Polavarapu, J. Feldmann, *ACS Catal.* **2018**, *8*, 3602.
- [2] a) Z. Li, W. Luo, M. Zhang, J. Feng, Z. Zou, *Energy Environ. Sci.* **2013**, *6*, 347; b) C. Martinez Suarez, S. Hernández, N. Russo, *Appl. Catal. A* **2015**, *504*, 158; c) Y. Park, K. J. McDonald, K.-S. Choi, *Chem. Soc. Rev.* **2013**, *42*, 2321; d) K. Tolod, S. Hernández, N. Russo, *Catalysts* **2017**, *7*, 13.
- [3] F. F. Abdi, N. Firet, R. van de Krol, *ChemCatChem* **2013**, *5*, 490.
- [4] a) X. Shi, H. Jeong, S. J. Oh, M. Ma, K. Zhang, J. Kwon, I. T. Choi, I. Y. Choi, H. K. Kim, J. K. Kim, J. H. Park, *Nat. Commun.* **2016**, *7*, 11943; b) Y. Pihosh, I. Turkevych, K. Mawatari, J. Uemura, Y. Kazoe, S. Kosar, K. Makita, T. Sugaya, T. Matsui, D. Fujita, M. Tosa, M. Kondo, T. Kitamori, *Sci. Rep.* **2015**, *5*, 11141; c) P. Chakthranont, T. R. Hellstern, J. M. McEnaney, T. F. Jaramillo, *Adv. Energy Mater.* **2017**, *7*, 1701515; d) Y. Qiu, W. Liu, W. Chen, W. Chen, G. Zhou, P.-C. Hsu, R. Zhang, Z. Liang, S. Fan, Y. Zhang, Y. Cui, *Sci. Adv.* **2016**, *2*, e1501764.
- [5] W. Luo, Z. Yang, Z. Li, J. Zhang, J. Liu, Z. Zhao, Z. Wang, S. Yan, T. Yu, Z. Zou, *Energy Environ. Sci.* **2011**, *4*, 4046.
- [6] T. W. Kim, K.-S. Choi, *Science* **2014**, *343*, 990.
- [7] a) S. J. A. Moniz, S. A. Shevlin, D. J. Martin, Z.-X. Guo, J. Tang, *Energy Environ. Sci.* **2015**, *8*, 731; b) X. Chang, T. Wang, P. Zhang, J. Zhang, A. Li, J. Gong, *J. Am. Chem. Soc.* **2015**, *137*, 8356; c) L. Zhang, E. Reisner, J. J. Baumberg, *Energy Environ. Sci.* **2014**, *7*, 1402.
- [8] a) D. K. Zhong, S. Choi, D. R. Gamelin, *J. Am. Chem. Soc.* **2011**, *133*, 18370; b) Y. H. Lai, D. W. Palm, E. Reisner, *Adv. Energy Mater.* **2015**, *5*, 1501668.
- [9] A. J. E. Rettie, H. C. Lee, L. G. Marshall, J.-F. Lin, C. Capan, J. Lindemuth, J. S. McCloy, J. Zhou, A. J. Bard, C. B. Mullins, *J. Am. Chem. Soc.* **2013**, *135*, 11389.
- [10] C. Zachäus, F. F. Abdi, L. M. Peter, R. van de Krol, *Chem. Sci.* **2017**, *8*, 3712.
- [11] M. Rohloff, B. Anke, S. Zhang, U. Gernert, C. Scheu, M. Lerch, A. Fischer, *Sustainable Energy Fuels* **2017**, *1*, 1830.
- [12] L. Chen, F. M. Toma, J. K. Cooper, A. Lyon, Y. Lin, I. D. Sharp, J. W. Ager, *ChemSusChem* **2015**, *8*, 1066.
- [13] J. K. Cooper, S. Gul, F. M. Toma, L. Chen, P.-A. Glans, J. Guo, J. W. Ager, J. Yano, I. D. Sharp, *Chem. Mater.* **2014**, *26*, 5365.
- [14] G. Park, J. Y. Park, J. H. Seo, K. H. Oh, A. Ma, K. M. Nam, *Chem. Commun.* **2018**, *54*, 5570.
- [15] J. Su, C. Liu, D. Liu, M. Li, J. Zhou, *ChemCatChem* **2016**, *8*, 3279.
- [16] S. Hernández, G. Gerardi, K. Bejtka, A. Fina, N. Russo, *Appl. Catal., B* **2016**, *190*, 66.
- [17] a) M. Veith, *J. Chem. Soc., Dalton Trans.* **2002**, 2405; b) M. Mehring, *Coord. Chem. Rev.* **2007**, *251*, 974.
- [18] a) J. Tucher, L. C. Nye, I. Ivanovic-Burmazovic, A. Notarnicola, C. Streb, *Chem. Eur. J.* **2012**, *18*, 10949; b) J. Tucher, K. Peuntinger, J. T. Margraf, T. Clark, D. M. Guldi, C. Streb, *Chem. Eur. J.* **2015**, *21*, 8716.
- [19] a) J. W. Pell, W. C. Davis, H. C. zur Loye, *Inorg. Chem.* **1996**, *35*, 5754; b) J. H. Thurston, T. O. Ely, D. Trahan, K. H. Whitmire, *Chem. Mater.* **2003**, *15*, 4407.
- [20] J. A. Seabold, K.-S. Choi, *J. Am. Chem. Soc.* **2012**, *134*, 2186.
- [21] M. Veith, S. Mathur, H. Shen, N. Lecerf, S. Hüfner, M. H. Jilavi, *Chem. Mater.* **2001**, *13*, 4041.
- [22] a) A. Walsh, Y. Yan, M. N. Huda, M. M. Al-Jassim, S.-H. Wei, *Chem. Mater.* **2009**, *21*, 547; b) D. J. Payne, M. D. M. Robinson, R. G. Egdell, A. Walsh, J. McNulty, K. E. Smith, L. F. J. Piper, *Appl. Phys. Lett.* **2011**, *98*, 212110.
- [23] L. Chen, E. Alarcón-Lladó, M. Hettick, I. D. Sharp, Y. Lin, A. Javey, J. W. Ager, *J. Phys. Chem. C* **2013**, *117*, 21635.
- [24] F. F. Abdi, R. van de Krol, *J. Phys. Chem. C* **2012**, *116*, 9398.
- [25] X. Shi, I. Y. Choi, K. Zhang, J. Kwon, D. Y. Kim, J. K. Lee, S. H. Oh, J. K. Kim, J. H. Park, *Nat. Commun.* **2014**, *5*, 4775.
- [26] a) A. Luque, S. Hegedus, *Handbook of Photovoltaic Science and Engineering*, 2nd ed., John Wiley & Sons Ltd, Chichester, UK **2011**; b) V. Andrei, R. L. Z. Hoye, M. Crespo-Quesada, M. Bajada, S. Ahmad, M. De Volder, R. Friend, E. Reisner, *Adv. Energy Mater.* **2018**, *8*, 1801403.
- [27] a) C. Carver, Z. Ulissi, C. K. Ong, S. Dennison, G. H. Kelsall, K. Hellgardt, *Int. J. Hydrogen Energy* **2012**, *37*, 2911; b) A. Hankin, F. E. Bedoya-Lora, C. K. Ong, J. C. Alexander, F. Petter, G. H. Kelsall, *Energy Environ. Sci.* **2017**, *10*, 346; c) A. Shinde, D. Guevarra, G. Liu, I. D. Sharp, F. M. Toma, J. M. Gregoire, J. A. Haber, *ACS Appl. Mater. Interfaces* **2016**, *8*, 23696; d) X. Yao, D. Wang, X. Zhao, S. Ma, P. S. Bassi, G. Yang, W. Chen, Z. Chen, T. Sritharan, *Energy Technol.* **2018**, *6*, 100.
- [28] W. J. Lee, P. S. Shinde, G. H. Go, E. Ramasamy, *Int. J. Hydrogen Energy* **2011**, *36*, 5262.